



OPEN ACCESS

EDITED BY

Elva G. Escobar-Briones,
National Autonomous University of Mexico,
Mexico

REVIEWED BY

Yuan-Pin Chang,
National Sun Yat-sen University, Taiwan
Luigi Jovane,
University of São Paulo, Brazil
Sandor Mulsow,
Austral University of Chile, Chile

*CORRESPONDENCE

Kiho Yang

✉ kyang@pusan.ac.kr

RECEIVED 15 August 2024

ACCEPTED 04 October 2024

PUBLISHED 22 October 2024

CITATION

An H, Jung J, Hwang H, Kim S, Kim J, Ko Y and Yang K (2024) Uncovering the oxic-suboxic microenvironment change in seamount flank through authigenic clay minerals in basaltic substrate of ferromanganese crust, Magellan seamount. *Front. Mar. Sci.* 11:1481396. doi: 10.3389/fmars.2024.1481396

COPYRIGHT

© 2024 An, Jung, Hwang, Kim, Kim, Ko and Yang. This is an open-access article distributed under the terms of the [Creative Commons Attribution License \(CC BY\)](https://creativecommons.org/licenses/by/4.0/). The use, distribution or reproduction in other forums is permitted, provided the original author(s) and the copyright owner(s) are credited and that the original publication in this journal is cited, in accordance with accepted academic practice. No use, distribution or reproduction is permitted which does not comply with these terms.

Uncovering the oxic-suboxic microenvironment change in seamount flank through authigenic clay minerals in basaltic substrate of ferromanganese crust, Magellan seamount

Hyeonho An^{1,2}, Jaewoo Jung², Huijeong Hwang³, Suhyun Kim¹, Jonguk Kim², Youngtak Ko² and Kiho Yang^{1,4*}

¹Department of Oceanography, Pusan National University, Busan, Republic of Korea, ²Ocean Georesources Research Department, Korea Institute of Ocean Science and Technology, Busan, Republic of Korea, ³School of Earth Sciences and Environmental Engineering, Gwangju Institute of Science and Technology, Gwangju, Republic of Korea, ⁴Institute for Future Earth, Pusan National University, Busan, Republic of Korea

In low-temperature ocean environments, basalt alteration by seawater precipitates authigenic clay minerals that serve as proxies for reconstructing paleo-ocean conditions because they reflect surrounding oxic-suboxic conditions. In this study, alteration rims on basaltic substrate associated with ferromanganese (Fe-Mn) crust from the Magellan seamount KC-7 were identified by microscopic analyses. Mineralogical and geochemical analyses indicate that the alteration rims contain K-enriched Fe-smectite and glauconite which suggest that seawater-basalt interaction occurred under oxic conditions and in the presence of organic-rich suboxic conditions, respectively. These disparate environmental conditions suggest that the environment changed before and after Fe-Mn crusts formed. During the Cenozoic hyperthermal events, oxygen-rich bottom water was supplied by upwelling driven by the geomorphological influence of the seamounts, which may have led to basalt alteration. The K-enriched Fe-smectites, which indicate oxic condition, formed via seawater-basalt interactions before the Fe-Mn crust incrustation. Later, during the Eocene, the opening of the Drake Passage enhanced the supply of oxygen-rich seawater to the Magellan Seamounts, thereby enabling the formation of hydrogenetic Fe-Mn crust. After the incrustation of seamount flanks with Fe-Mn crusts, the carbonate fluorapatite (CFA), a product of the global phosphatization event, filled the pores in the Fe-Mn crusts during Oi-1 glaciation. As a result, seawater-basalt interactions decreased and led to suboxic conditions, in which glauconite formed as organic matter was remineralized under the organic-rich

conditions in the basaltic substrate. This authigenic clay mineral formation sequence suggests that changes in ocean circulation and subsequent changes in the oxic-suboxic conditions in the basaltic substrate occurred on the western Pacific seamount KC-7.

KEYWORDS

ferromanganese crust, authigenic phyllosilicate, western pacific seamount, paleocean environment reconstruction, seawater-basalt alteration, drake passage opening

1 Introduction

The Magellan seamounts were formed in the Southern Hemisphere during the Cretaceous, approximately 87 Ma (Glasby et al., 2007; Hyeong et al., 2013), and moved to the western Pacific Ocean owing to the tectonic motions of the Pacific Plate (Menard, 1984; Duncan and Clague, 1985; Hyeong et al., 2008). The Pacific Plate moved northward during the period 76–43 Ma then shifted to northwestward motion at a latitudinal rate of 0.3°/Ma (Wessel and Kroenke, 1998; Hyeong et al., 2008). Seamount KC-7 comprises basalt, phosphorite, and limestone, and its flanks are covered by Fe-Mn crusts (Melnikov and Pletnev, 2013). Seamount KC-7 was located near the paleo-equator at approximately 57 Ma (Hyong et al., 2008), during the Paleocene-Eocene Thermal Maximum (PETM). Since the Eocene, Fe-Mn crusts formed and eventually coating the seamount flanks (Glasby et al., 2007). The growth of Fe-Mn crusts depends on well-developed oxygen minimum zone (OMZ) (Glasby et al., 2007), as the supply of oxygen-rich seawater oxidizes dissolved Mn and Fe, precipitating Fe-Mn oxides. Seamounts, as structures that obstruct the flow of bottom water, induce upwelling (Eriksen, 1991; McClain, 2007), which allows for the supply of oxygen-rich bottom water to the seamount flanks (Pitcher et al., 2007). The supply of oxygen-rich seawater in the Pacific Ocean is likely related to the opening of the Drake Passage (approximately 49 Ma), which started influencing the Pacific at approximately 41 Ma (Livermore et al., 2005; Scher and Martin, 2006; Toumoulin et al., 2020). The opening of the Drake Passage likely facilitated the formation of Antarctic Bottom Water (AABW) alongside the enhancement of the Antarctic Circumpolar Current (ACC) (Shao et al., 2013; Hutchinson et al., 2021), and the formation of Fe-Mn crusts is associated with this oxygen-rich deep current (Wu et al., 2007; Koschinsky and Hein, 2017).

Low-temperature alteration of basalt controls the elemental cycling between the lithosphere and hydrosphere (Jarrard, 2003; Yamashita et al., 2019; Ramos et al., 2020). Alteration processes such as oxidation, hydration, and alkali fixation result in the formation of secondary minerals (Alt and Honnorez, 1984; Alt et al., 1986; Jarrard, 2003). Clay minerals and Fe-oxyhydroxide formation is a ubiquitous process in such environments (Yang et al., 2018), and the chemical composition and structure of

authigenic phyllosilicates formed by alteration reflect their formation environment (Yang et al., 2016, 2018) and mechanisms, which vary based on the fluid composition and oxidizing conditions (Pichler et al., 1999; Wilson, 1999). Thus, clay minerals have been used as proxies for paleo-ocean environmental reconstruction (Yang et al., 2016, 2018; Jung et al., 2022; Kim et al., 2023). K-enriched Fe-smectite and glauconite are clay minerals that indicate oxic and suboxic conditions, respectively, during basalt alteration (López-Quirós et al., 2019). Generally, Fe-smectite forms by the hydrothermal alteration of basalt (Dekov et al., 2008; Cuadros et al., 2011), whereas K-enriched Fe-smectite forms via seawater alteration of basalt (Clayton and Pearce, 2000; Yamashita et al., 2019). Fe-oxyhydroxide forms as secondary minerals in the oceanic crust (Edwards et al., 2005; Knowles et al., 2012) and have been identified based on clay minerals in low-temperature oxic environments (Bach and Edwards, 2003). Glauconite occurs in marine sediment as terrigenous-allogenic or authigenic types (Logvinenko, 1982; Baldermann et al., 2022). Authigenic glauconite forms via glauconitization in partially suboxic micro-environments, which occurs in organic-rich settings that contain the precursor Fe-smectite (Odin and Matter, 2003; Baldermann et al., 2013; López-Quirós et al., 2019). In addition, glauconite can form as a secondary mineral in the deep sea via interactions between pillow basalt and seawater (Böhlke et al., 1980). This suggests that glauconite found in basaltic substrate associated with Fe-Mn crust reflects the formation of secondary minerals as a result of basalt alteration in a partially suboxic micro-environment.

Previous studies have suggested that global climate change was influenced by the Drake Passage opening during the Eocene using geographic and $p\text{CO}_2$ modeling (Toumoulin et al., 2020), $\delta^{18}\text{O}$ records from benthic foraminifera (Livermore et al., 2005), and seawater Nd isotope compositions (Scher and Martin, 2006). Paleoenvironmental reconstructions related to the opening of the Drake Passage using clay minerals have generally focused on the Antarctic region (Ehrmann and Mackensen, 1992). Moreover, owing to its potential of Fe-Mn crusts as prospective mining targets, previous studies have investigated the ages of the Fe-Mn oxide layers (Halbach and Puteanus, 1984; Puteanus and Halbach, 1988; Kim et al., 2006), formation mechanisms, and phosphatization episodes (Hyong et al., 2008, 2013; Melnikov and Pletnev, 2013; Yang et al., 2019). However, few studies have

utilized authigenic phyllosilicates formed in the basaltic substrate of Fe-Mn crusts, part of seamounts, to reconstruct paleo-ocean environments. The Magellan Seamounts in the western Pacific have experienced prolonged water-rock interactions and oceanographic changes. In this study, we analyzed the mineralogy and geochemistry of clay minerals in the basaltic substrate associated with Fe-Mn crusts to identify changes induced by the formation of the Fe-Mn crusts on the seamount flanks. We hypothesized that the formation of the Fe-Mn crust may have weakened the seawater-basalt interactions on the seamount flanks. As the Fe-Mn crust developed over the basaltic substrate on the seamount flanks, it likely acted as a barrier, limiting further direct contact between seawater and the underlying basalt. To address this, we analyzed the Fe-Mn layers and basaltic substrate from seamount KC-7 in the Magellan Seamount cluster. Paleo-oceanographic changes, such as the incrustation of Fe-Mn crusts, likely influenced the oxic-suboxic conditions on the seamount flanks. For this reason, this approach was applied in paleo-oceanographic reconstruction. The reconstruction of oxic-suboxic conditions on western Pacific seamounts obtained herein can be used to understand the impacts of climate change on ocean environments.

2 Material and methods

2.1 Sample collection and preparation

The Fe-Mn crust sample DGCR1314U01 from KC-7 in the Magellan Seamount cluster (Figure 1) was recovered using a dredge line from 16°54.869'N and 151°50.030'E to 16°55.152'N and 151°50.220'E (length: approximately 0.62 km; depth: 1536–1523 mbsl) during the CR1302 expedition (Korea Institute of Ocean Science & Technology, February 14–March 13, 2014; R/V *Onnuri*). The approximately 104 mm thick Fe-Mn oxide layers were divided

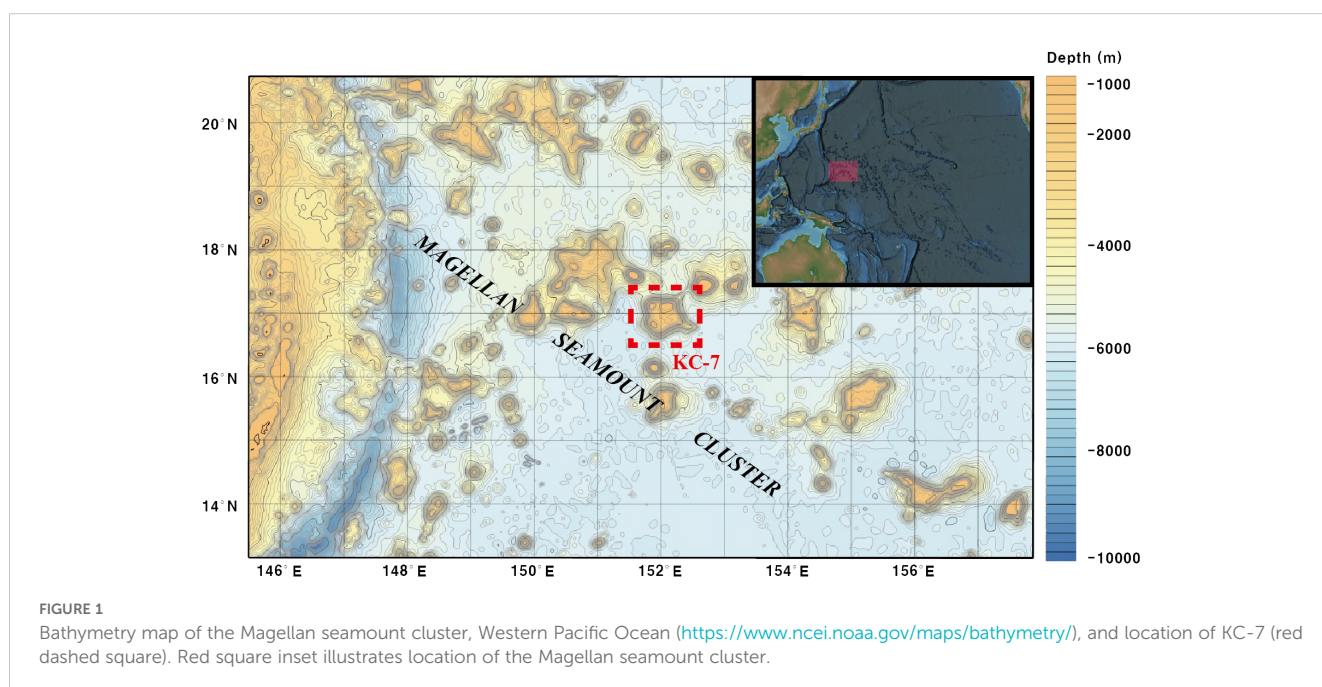
into seven distinct layers by optical observation, which included a highly altered basaltic substrate. Co chronometry (Manheim and Lane-Bostwick, 1988; Puteanus and Halbach, 1988) using modified empirical equation (Equation 1 in supplementary) (Moon, 2016) dated the age of the lowest Fe-Mn oxide layer at 40.78 Ma, with an average growth rate of approximately 2.60 mm/Ma observed for the middle Eocene (Supplementary Tables S1, S2). Dating was performed at one or two points in the middle of each distinct layer to minimize the influence of layer boundary inclination. Fe-Mn crust samples were halved, and powder samples obtained each layer using a microdrill with a tungsten carbide carving bit (Dremel 3000, Ø=0.8 mm), which was then consolidated using Akasel Aka-Resin liquid epoxy and polished using sandpaper. Thin sections were then prepared for geochemical and mineralogical analysis of the basaltic substrate and the lowest part of the Fe-Mn oxide layer.

2.2 Polarization microscopy

A Nikon ECLIPSE LV100N POL polarization microscope at the Korea Institute of Ocean Science & Technology (KIOST), Busan, Republic of Korea was used to examine thin sections of the basaltic substrate. Open and crossed Nicol prism conditions were used for optical observation and mineral identification.

2.3 X-ray diffraction analyses

Powder samples were obtained using a microdrill and immersed in distilled water in a sonicator to minimize flocculation (Yang et al., 2019). The oriented samples were then placed on glass slides. To determine the mineralogy of the Fe-Mn crust and basaltic substrate, X-ray Diffraction (XRD) was performed using a PAN analytical X'pert Pro system at KIOST, under the conditions of 45 kV and 30



mA and a $\text{CuK}\alpha$ radiation source. The receiving slit was set to $>0.2^\circ$ to optimize the resolution of the XRD profile and the peak intensity (Hurst et al., 1997; Jung et al., 2022). XRD profiles were obtained over a 2θ range of $4\text{--}60^\circ$ at scan speed of $1.2^\circ/\text{min}$ and a scan step size of 0.02° , and mineral composition was determined using the *Crystallographica Search-Match* software (version 2.0.3.1).

2.4 Micro X-ray fluorescence analyses

Elemental Al, Si, K, and Fe compositions were measured using the Bruker M4 Tornado μ -XRF at the Korea Institute of Industrial Technology, Wonju, Republic of Korea. Analysis was performed using Rh anode tube at 50 kV and collection time of 1 s. Element distribution maps were constructed using geochemical analysis of the basaltic substrate in the Fe-Mn crust, which was performed in 0.025 mm steps with a count time of 600 ms per point. Built-in XRF software (Bruker XRF, Germany) was used for the quantitative analysis of each element.

2.5 Field emission scanning electron microscopy

Microscopic and geochemical analyses were performed using thin sections coated with Pt. Sections were examined using the ZEISS Gemini 500 field emission scanning electron microscope (FE-SEM) at an acceleration voltage of 10 kV and working distance of 5 mm and by energy dispersive X-ray spectrometry (EDS) at an acceleration voltage of 15 kV and a working distance of 8.5 mm. Analysis was performed at the Pusan National University, Busan, Republic of Korea. Backscattered electron (BSE) images were obtained for chemical distinction of the alteration rims and the groundmass. EDS was used to examine the chemical composition of the distinct alteration rims.

2.6 Micro Raman spectroscopy

Micro Raman spectroscopy was conducted using a Ramboss star micro-Raman system (DXG) at the Gwangju Institute of Science and Technology, Gwangju, Republic of Korea. A 785 nm laser source (>90 mW) was used to ascertain the clay mineral composition of the alteration rims in the basaltic substrate. Raman spectra were collected with a spectral resolution of $\sim 0.24\text{ cm}^{-1}$ using a 1200 gr/mm grating, with both the lower wavenumber ($27\text{--}1230\text{ cm}^{-1}$) and the hydroxyl-stretching regions ($3446\text{--}3711\text{ cm}^{-1}$) examined. The laser power on the sample was operated through a 0.40 NA, 20x objective at about 28.5 mW. Each Raman spectrum was obtained as an average of 10 spectra recorded over 10 s. Spectra were cross-referenced against spectral mineral patterns in the laboratory collection and databases available through *CrystalSleuth* provided by RRUFF for comparison. Spectrometer calibration was performed using the Raman band for a silicon wafer at 520 cm^{-1} (Bernardini et al., 2024). The measured spectrum was baseline corrected and fitted with Voigt function to obtain the phonon wavenumbers and intensities.

2.7 Transmission electron microscopy

Samples for TEM were obtained from the alteration rim of the thin section using an FEI Scios DualBeam focused ion beam. Samples were placed on a holey-carbon TEM Cu grid (TED PELLA Inc.) and a TALOS F200X field-emission transmission electron microscope at Pusan National University was used to identify the microstructure and chemical composition of the clay minerals. TEM was performed at 200 kV to examine the clay minerals on the lattice fringes and for EDS analysis. Bright-field TEM images and fast Fourier transform (FFT) images were evaluated by *Gatan digital micrograph* software (version 3.01.598.0, Gatan Inc.) to identify the d-spacing of the lattice fringes and analyze the microstructures of the clay minerals. The chemical formula of the smectites was calculated as atoms per formula unit (apfu) based on $\text{O}_{20}(\text{OH})_4$. To identify the different types of smectites, the octahedral chemical compositions were plotted on an $^{\text{VI}}\text{Al}\text{--Fe}\text{--Mg}$ ternary diagram that included saponite (Mg-rich), montmorillonite-beidellite (Al-rich), and nontronite (Fe-rich) domains (Weaver, 1989; Marinoni et al., 2008; Jung et al., 2022).

3 Results

3.1 Features of the basaltic substrate and Fe-Mn crust


Visual observation showed that the Fe-Mn crusts are divided into seven layers, including a basaltic substrate. The texture of the upper layers 1–3 was porous and infilled with sediments (Table 1), while the lower layers 4–6 exhibited more common characteristics of a relatively blocky texture. Both texture differentiation and distinct colors were observed in the layers (Table 1). L1 (at the crust surface) was a reddish-brown color and 23 mm thick; L2 was dark brown and ~ 18 mm thick; L3 was yellowish brown and ~ 20 mm thick; L4 was dark gray and ~ 13 mm thick; L5 was a gray layer with white chunks and ~ 15 mm thick; and L6 was light gray in color with white chunks and ~ 15 mm thick (Table 1). The upper Fe-Mn layers were dated to approximately 19.18–2.84 Ma and the lower layers to approximately 40.78–26.45 Ma (Table 1).

The highly altered basaltic substrate (Ba) included dark green matrix material, in which micro-XRF analysis confirmed relatively high Si, Al, and K contents (Figure 2), and a light-yellow matrix (Figure 3). Greenish-brown alteration rims were observed in the dark green matrix (Figure 3A) and traces of planktonic foraminifera (*Globorotalia menardii*) in the light-yellow matrix (Figure 3B).

3.2 Geochemistry and mineralogy of the Fe-Mn crust

Diffraction patterns of bulk powder samples from each layer (L1–Ba) were examined to obtain the mineral assemblage of the air-dried samples (Figure 4). Manganese oxide minerals, identified as vernadite ($\delta\text{-MnO}_2$), were observed in all manganese layers,

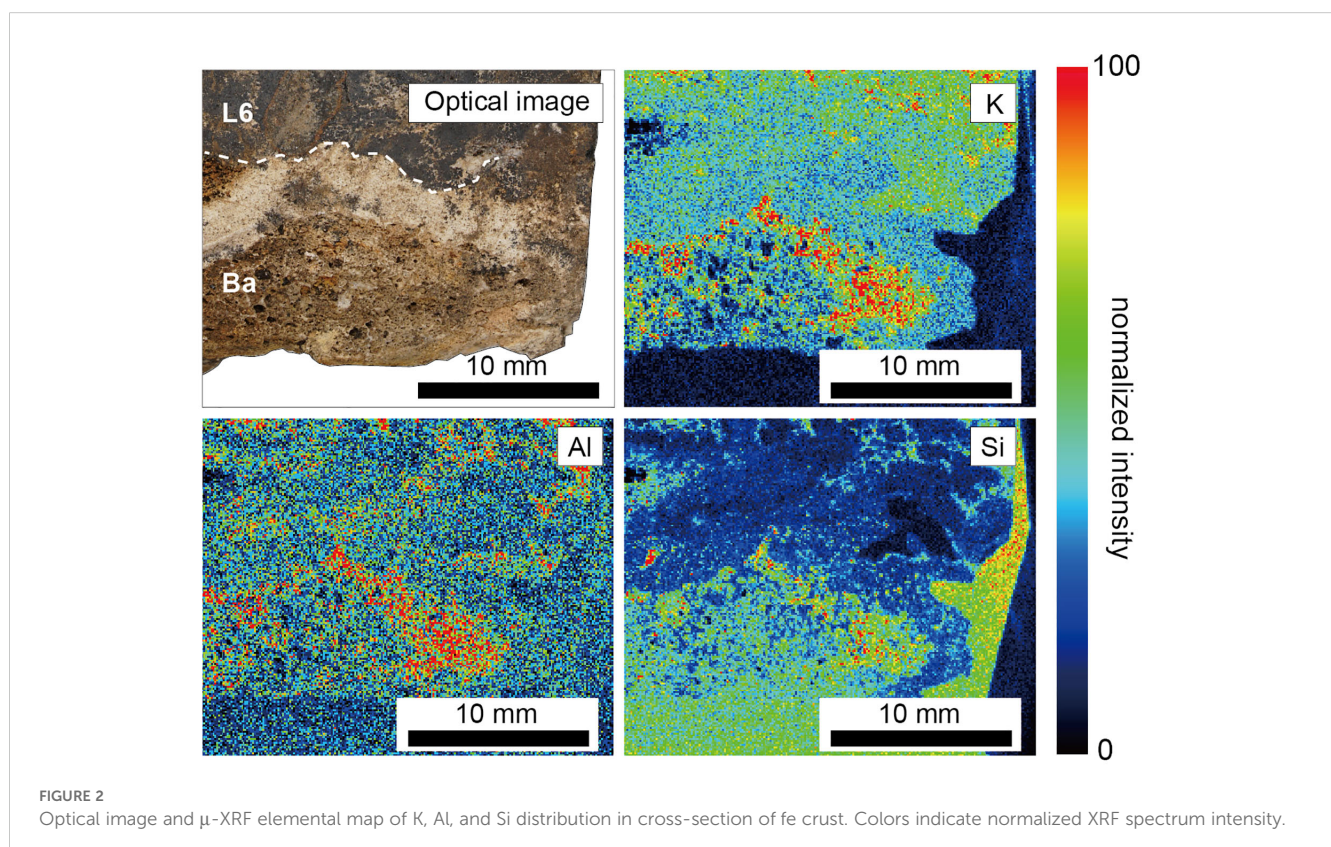
TABLE 1 Summary of layer thickness, age, description, and mineralogy of the ferromanganese crust.

Optical Image	Layers	Thickness (mm)	Age (Ma)	Description	Major Mineralogy
	1	0 – 23	2.84 (5mm) 5.54 (15 mm)	Reddish brown, porous	vernadite (δ -MnO ₂)
	2	23 – 41	9.74, 13.10 (25, 35 mm)	Dark brown, porous	vernadite (δ -MnO ₂)
	3	41 – 61	15.10, 19.18 (45, 55 mm)	Yellowish brown, porous, sediments filled	vernadite (δ -MnO ₂)
	4	61 – 74	26.45 (67.5 mm)	Dark gray, blocky layer	vernadite (δ -MnO ₂)
	5	74 – 89	30.17 (80 mm)	Gray, blocky layer with white chunks	vernadite (δ -MnO ₂), carbonate fluorapatite (CFA)
	6	89 – 104	33.39, 40.78 (90, 102.5 mm)	Light gray, blocky layer with white chunks	vernadite (δ -MnO ₂), carbonate fluorapatite (CFA)
	Ba	104 – 113	Light yellow and dark green with greenish brown rims Highly altered phosphorite cemented porous basaltic substrate	Carbonate fluorapatite (CFA)	

appearing as a broad peak at 2θ of 36.6° , while distinct carbonate fluorapatite (CFA) was identified in the lower part of the Fe-Mn crust, L5–Ba (Figure 4).

Several differences between the substrate matrix and alteration rims were observed in the BSE images and elemental maps

(Figures 5A–H). The matrix exhibited high concentrations of P (average 14.93 wt. %) and Ca (average 31.77 wt.%) while showing relatively low Si (average 0.24 wt.%) and Al (0.03 wt.%) (Figures 5B, C). The alteration rims showed higher Si concentrations (average of 21.13 wt. %) and Al (average 8.66 wt.%) compared to the matrix



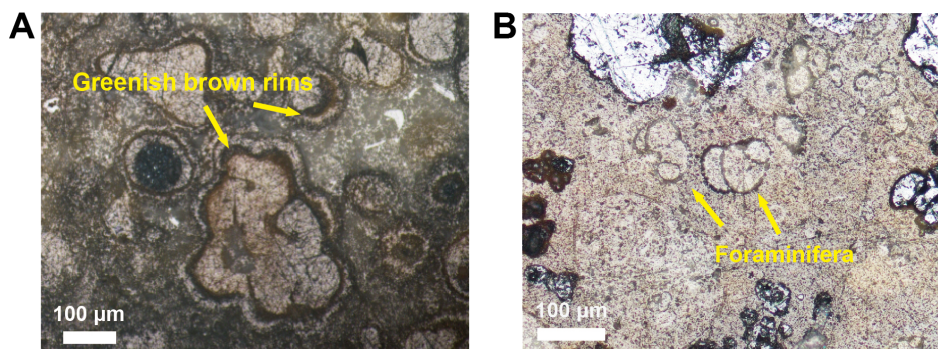


FIGURE 3

Optical images of thin section from the basaltic substrate obtained using a polarization microscope under open nicol prism conditions. (A) Dark green matrix with greenish brown alteration rims. (B) Light yellow matrix including *Globorotalia menardii* (*G. menardii*).

(Figures 5D, E), along with relatively higher K (average 3.33 wt.%), Mg (average 2.28 wt.%), and Fe (average 9.40 wt.%) contents (Figures 5D–H). These chemical compositions suggest that the alteration rims are likely composed of clay minerals.

The quantitative analysis results of the metal elements in the manganese oxide of layer 6 were plotted on a Fe-Mn-(Co + Ni + Cu) ternary diagram (Bonatti, 1972), with the plot showing the

distribution of the manganese oxide elements corresponding to the hydrogenetic domain (Figure 6).

3.3 Results of micro Raman analyses of alteration rim

Raman spectroscopy offers significant advantages in identifying specific types of clay minerals that are often undetectable (or indistinguishable) by X-ray diffraction measurements. The Raman spectrum measured for the alteration rim within the 250–600 cm^{-1} spectral region shows two distinct broad bands with 250–450 cm^{-1} and 450–575 cm^{-1} (Figure 7). This spectral region includes the complexation of two clay minerals, identified as nontronite and glauconite, by comparison with the reference Raman spectra X050120 (Nontronite) and R070295 from the RRUFF database. The observed spectral band between 250 and 450 cm^{-1} is fitted using four distinct bands. The Raman bands at approximately 356 and 418 cm^{-1} are attributed to the vibrations of SiO_4 in nontronite (Frost and Klopogge, 2000). Other bands at 335 and 388 cm^{-1} were assigned to glauconite, with the 388 cm^{-1} band being the most prominent for glauconite when using a red laser (Coccatto et al., 2016). For 450–575 cm^{-1} spectral region, the observed band was deconvoluted with three spectral bands. The first band at 502 cm^{-1} is assigned to nontronite, while the bands appeared 526 cm^{-1} and 544 cm^{-1} are attributed to glauconite. The Raman spectra results indicate that nontronite and glauconite are the main clay mineral components of the alteration rim in the basaltic substrate, which consistent with the elemental analysis.

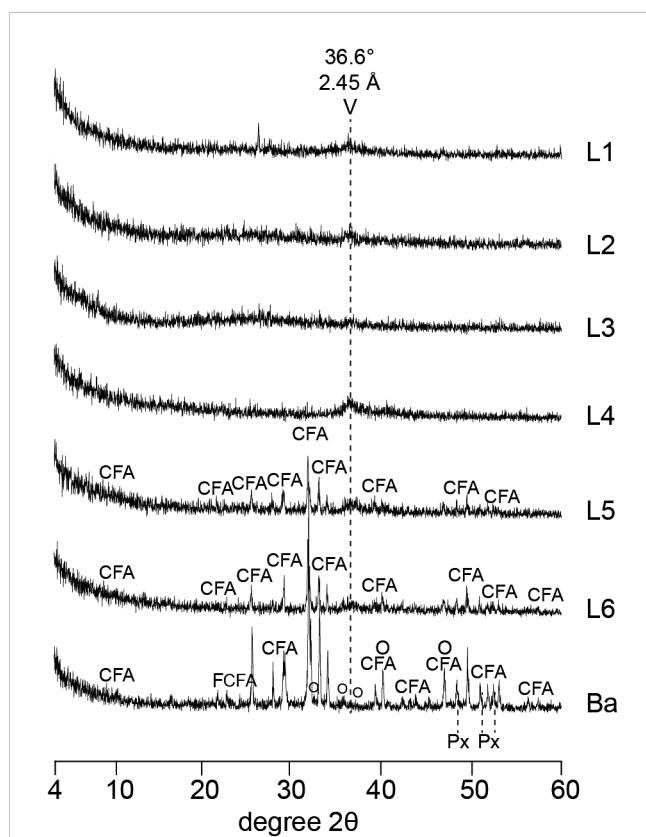


FIGURE 4

XRD profiles of air-dried powder samples (Q, quartz; V, vernadite; O, olivine; Px, pyroxene; CFA, carbonate fluorapatite). Vernadite ($\delta\text{-MnO}_2$) is present in all manganese layers (L1–L6), while CFA is observed only in the lower layers (L5–Ba). Ba: basaltic substrate.

3.4 Microscopic analyses of clay minerals in basaltic substrate

The lattice fringes in the EDS spectrum were observed using a representative TEM bright-field micrograph, with FFT images used to observe the clay minerals (Figures 8A, B). Clay minerals including chlorite with a 1.4 nm spacing, smectite with a 1.2 nm spacing, and mica with a 1.0 nm spacing, were observed. Smectite and mica were interlayered with Fe-oxyhydroxide with a 0.25 nm spacing (Figure 8A).

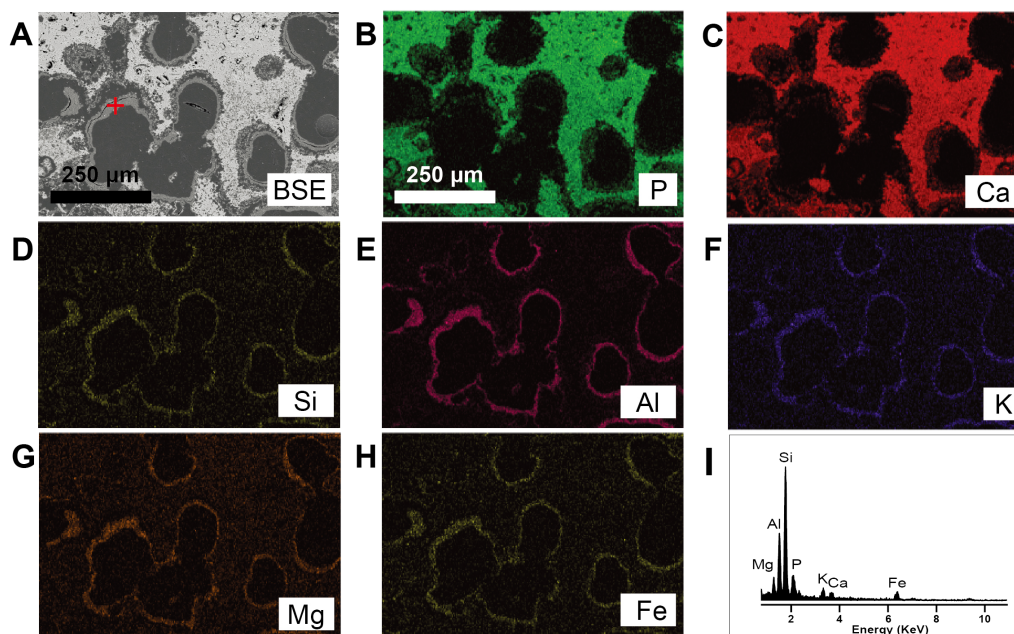


FIGURE 5
(A) BSE image. **(B–H)** Energy dispersive X-ray spectroscopy (EDS) elemental maps of basaltic substrate. Color intensity indicates elemental concentrations. **(B, C)** High concentrations of P and Ca in matrix. **(D–H)** High Si, Al, K, Mg, and Fe concentrations in alteration rims. **(I)** EDS spectrum of alteration rim (red-cross on BSE image).

The chemical composition of smectite was $[(K_{0.47-1.04})(Fe_{0.87-1.62}Al_{1.91-2.57}Mg_{0.72-1.55})(Al_{0.78-1.56}Si_{6.44-7.22})O_{20}(OH)_4]$ (Table 2), and the Al/Si ratio was between 0.34 and 0.50. The EDS results for the octahedral cation were plotted on an ^{VI}Al -Fe-Mg ternary diagram to compare the smectite group endmembers, confirming the presence of a Fe-smectite adjacent to the nontronite endmember (Figure 9A). The interlayer Fe-smectite showed K enrichment characteristics (Figure 9B), indicating that the smectite at the alteration rim of the basaltic substrate was K-enriched Fe-smectite.

4 Discussion

4.1 Formation of secondary phase minerals

Water-rock interactions that influence the global elemental cycles tend to form secondary minerals as products. In marine environments, these minerals form as a result of interactions between seawater and basalt at seamounts or in the oceanic crust (Jarrard, 2003; Yamashita et al., 2019; Ramos et al., 2020). In this

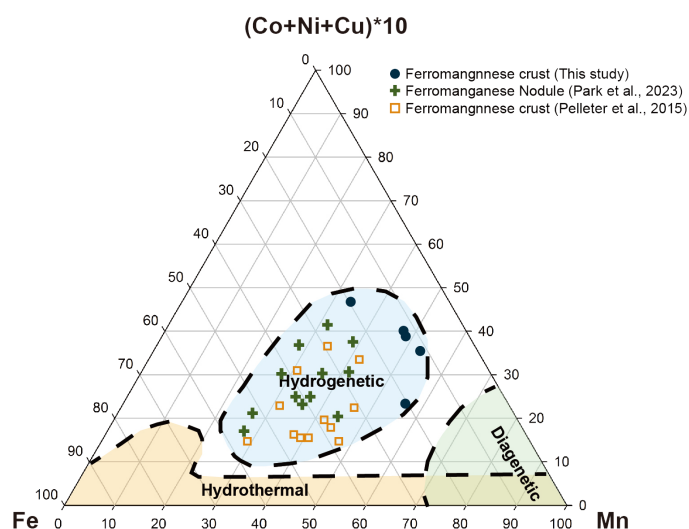
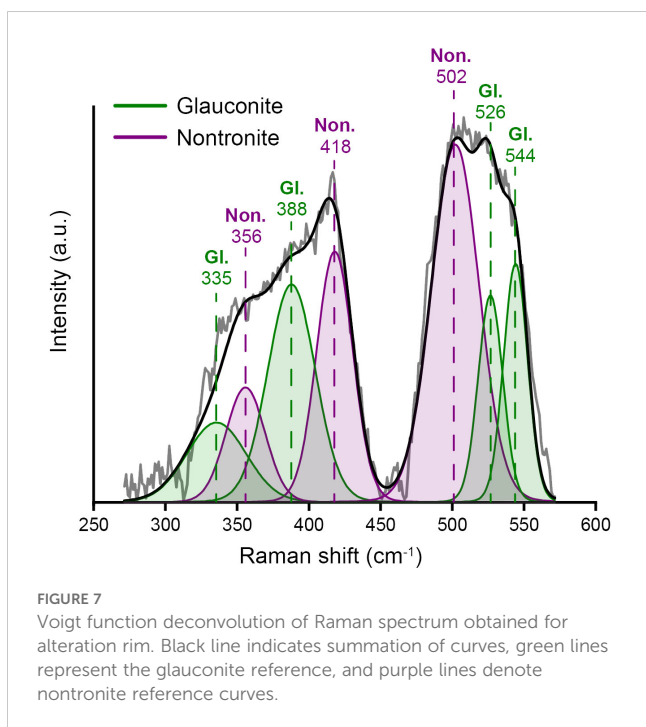


FIGURE 6
 Distribution of L6 minerals in the ternary plot for Fe–Mn–(Co + Ni + Cu) × 10 (modified from Bonatti, 1972). Closed circle represents L6 of ferromanganese crust from KC-7 (this study). Green crosses represent a ferromanganese nodule from KC-8 (Park et al., 2023) in the vicinity of KC-7, and open yellow squares denote ferromanganese crust from the southwestern Pacific (Pelletier et al., 2015).



study, secondary minerals were observed in the dark green areas of the basaltic substrate, in which relatively high Al, Si, and K concentrations were expected to lead to clay mineral formation (Figure 8). Furthermore, greenish-brown alteration rims indicative of clay minerals and are characterized by higher Al, Si, and K concentrations compared with those of the surrounding matrix were also identified in the dark green areas of the basaltic substrate (Figures 2, 5). Alteration rims were formed by the alteration of basalt via seawater-basalt interaction as fluids infiltrate veins or fractures (Alt and Honnorez, 1984). Since clay minerals are used as proxies for reconstructing paleo-ocean environments (Yang et al., 2016, 2018; Jung et al., 2022; Kim et al., 2023), the clay minerals in

the alteration rim can be used to reconstruct the oxic-suboxic conditions on seamount flanks prior to the formation of the Fe-Mn crust. However, identifying clay minerals in the samples using XRD (Figure 4) was challenging owing to the low abundance and poor crystallinity of the authigenic minerals. Micro Raman spectroscopy allowed for non-destructive analysis of material with poor crystalline characteristics. The micro Raman spectroscopy and TEM analyses confirmed the presence of smectite, and glauconite in the alteration rims (Figures 7, 8). Fe-smectite is generally observed in submarine environments in which basaltic glass has undergone low temperature hydrothermal alteration (Melson and Thompson, 1973; Alt et al., 1987; Yang et al., 2018; Yamashita et al., 2019). The Fe-smectite that forms in hydrothermal settings typically exhibits low Mg and K contents; however, the Fe-smectite on seamount KC-7 was relatively enriched in Mg and K characteristics (Figure 9). According to previous research (Yamashita et al., 2019), Si and Fe are derived from basalt dissolution during authigenic mineral formation resulting from seawater-basalt interactions, whereas Mg and K are derived from circulating seawater. Moreover, preferential K fixation in nontronite is the result of its large cell dimensions, which are compatible with larger ionic radius of K compared with those of Na and Ca (Meunier, 2005; Yamashita et al., 2019). Therefore, the Fe-smectite in the basaltic substrate of the Fe-Mn crust likely formed via interactions between oxygenated seawater and basalt before the incrustation of the Fe-Mn crust. Additionally, Fe-oxyhydroxides with a d-spacing of 0.25 nm (Figure 8) co-occurred with the Fe-smectite, indicating oxic conditions (Hein et al., 1979; Alt et al., 1987; Chevrier et al., 2007). Therefore, the Fe-smectite in the basaltic substrate formed in an environment in which oxygen was continually supplied by seawater circulation. A steady oxygen supply is necessary to form authigenic clay minerals in marine environments, whereas maintaining non-vigorous seawater circulation is crucial for preventing the dilution of Mg and K derived from seawater (Yamashita et al., 2019). Si and Fe likely originated from the

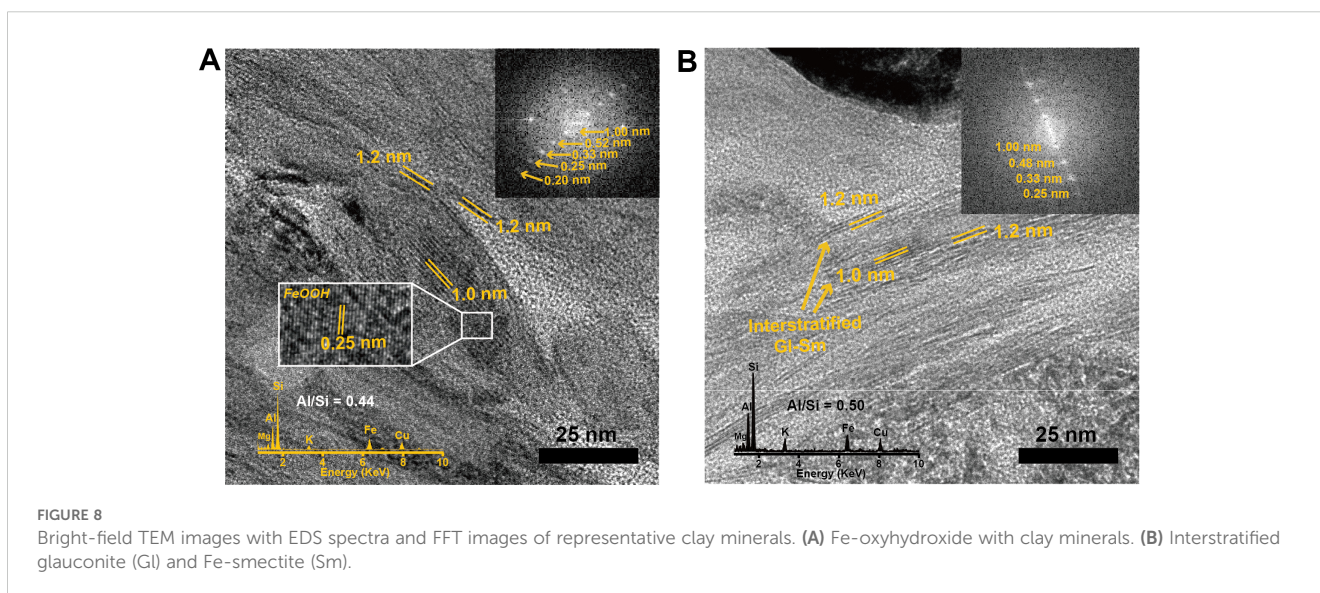


TABLE 2 Selected calculated chemical analysis results obtained for clay minerals based on $O_{20}(OH)_4$.

Analyses point	1	2	3	4	5	6
Si	6.44	6.78	7.13	6.64	6.78	7.22
^{IV} Al	1.56	1.22	0.87	1.36	1.22	0.78
Mg	1.11	0.98	1.06	1.03	0.72	1.55
Fe	1.62	1.21	1.38	0.93	0.99	0.87
^{VI} Al	1.91	2.28	1.97	2.57	2.51	2.07
K	0.47	0.57	0.62	0.69	1.04	0.60
Ca	0.01	0.02	0.03	0.00	0.00	0.02
Na	0.10	0.14	0.00	0.04	0.19	0.11
Al/Si	0.46	0.44	0.34	0.50	0.47	0.34
TC	-0.66	-0.76	-0.68	-0.72	-1.27	-0.75

Unit: atoms per formula unit (apfu).
TC, total charge.

basalt during seawater-basalt interactions, while K, Mg, and O were likely supplied by the non-vigorous seawater circulation driven by upwelling near the seamount flank. In other words, Fe-smectite authigenesis is expected to involve non-vigorous circulation of oxygenated seawater (Figure 10A).

Mica interstratified with Fe-smectite was identified as glauconite (Figure 7). The nature of glauconite is challenging owing to subtle differences (e.g., similar physical, chemical, and mineralogical characteristics) from other green clays (López-Quirós et al., 2020; Singh et al., 2023). Glauconite is predominantly a K- and Fe-rich mica that forms in suboxic conditions that typically occur in shallow marine environments (< 500 m) at around 15°C (Odin, 1988; López-Quirós et al., 2019, 2020). However, previous studies have suggested that glauconite forms in deep-sea environments (> 2000 m) at lower temperatures (3–6°C) (Giresse and Wiewióra, 2001; Cuadros et al., 2011; Baldermann et al., 2013; López-Quirós et al., 2019). Thus, the presence of glauconite suggests that the micro-

environment in the basaltic substrate may have transitioned from oxic to suboxic conditions (Figure 10B). The formation of glauconite on seamount flanks in suboxic micro-environmental conditions likely occurred after the Fe-Mn crust incrustation, as seawater-basalt interaction weakened owing to the global phosphatization event that formed the CFA (Benites et al., 2021; Hein et al., 2017). The porosity of hydrogenetic Fe-Mn crusts is approximately 60% (Conrad et al., 2017; Hein et al., 2017), and CFA is known to saturate the pores of Fe-Mn crusts (Yang et al., 2019). Therefore, CFA precipitation would have weakened seawater-basalt interaction and reduced the supply of oxygenated seawater. As a result, glauconite formation was likely promoted via the remineralization of organic matter and glauconitization in a suboxic micro-environment (López-Quirós et al., 2020). In other words, the presence of authigenic phyllosilicates formed by seawater-basalt interactions suggests that K fixation and Fe cycling occurred on the flanks of seamount KC-7 (Figure 10). The Fe-smectite likely formed in the basaltic substrate first, followed by glauconite, suggesting that the micro-environmental conditions in the basalt on the seamount flanks may have transitioned from oxic to suboxic conditions following the formation of the Fe-Mn crust.

4.2 Reconstruction of the paleo-ocean environments

4.2.1 Oxic condition in basaltic substrate

The western Pacific seamounts were located near the paleo-equatorial area approximately 57 Ma (Hyeong et al., 2008, 2013), which is almost simultaneous to the PETM (about 56 Ma), characterized by relatively slow ocean circulation and low dissolved oxygen concentrations (Tripathi and Elderfield, 2005; Winguth et al., 2012; Song et al., 2019). The maximum age of obtained from the Fe-Mn crust in this study was approximately 40.78 Ma; thus, it is possible that direct seawater-basalt interaction on flanks of seamount KC-7 during global hyperthermal events such as the PETM (56 Ma), early Eocene Climate Optimum (EECO;

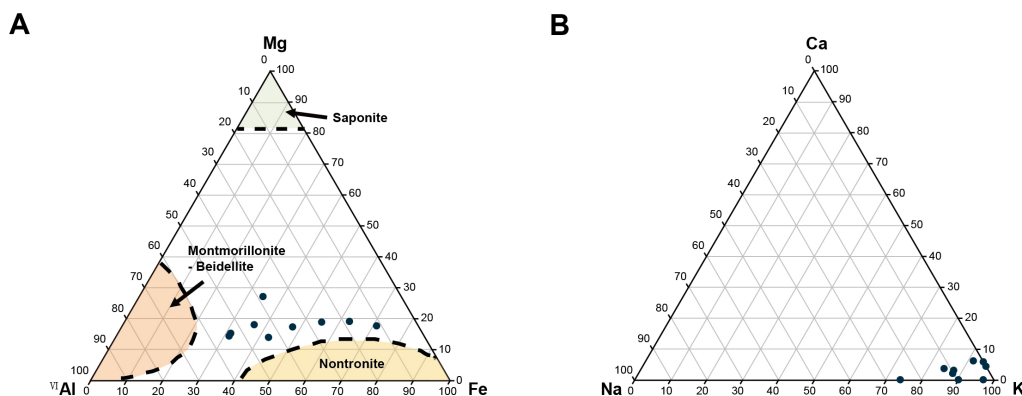


FIGURE 9 Ternary diagrams of Fe-smectite from the alteration rim, showing (A) octahedral, and (B) interlayer cations.

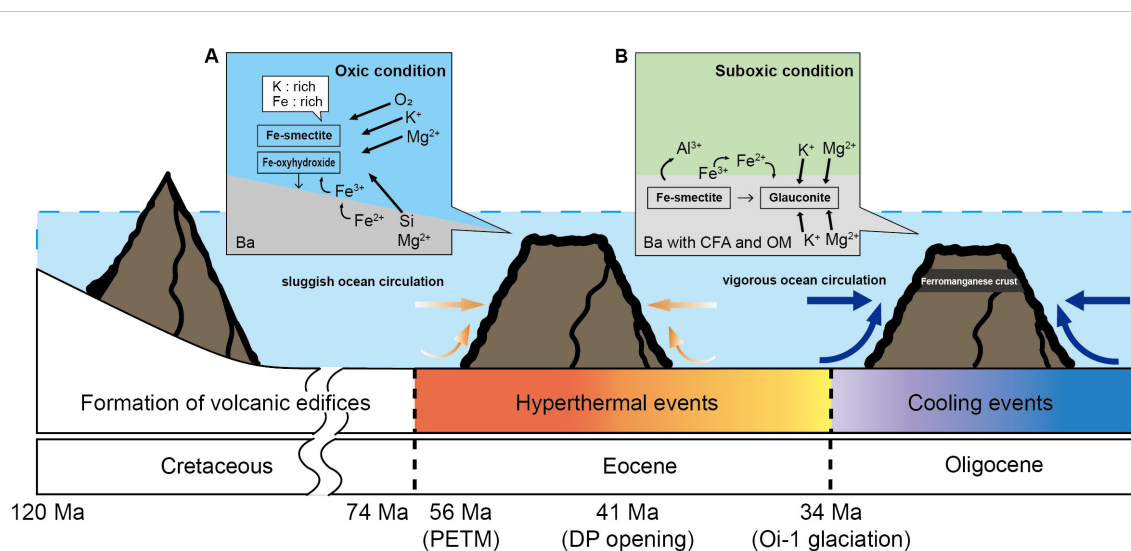


FIGURE 10

Schematic illustrations of authigenic phyllosilicate mineral formation on KC-7. (A) Fe-smectite formation under oxic conditions during the Eocene with sluggish ocean circulation. Geomorphological influence of the seamount as a result of upwelling along the flanks. The global ocean circulation intensified after the early Drake Passage opening around 41 Ma. (B) Glauconite formation process under suboxic conditions following cooling events. CFA blocked direct seawater-basalt interaction after the Oi-1 glaciation. DP, Drake Passage.

54–49 Ma), and middle Eocene Climate Optimum (MECO; 40 Ma) (Zeebe, 2013; Giorgioni et al., 2019; Scotese et al., 2021). These periods are characterized by slow ocean circulation and low dissolved oxygen concentration. However, upwelling driven by the geomorphological features of seamounts may have resulted in the supply of relatively oxygen-rich seawater to the seamount flanks (Figure 10). As a result, the precipitation of Fe-smectite in basaltic substrate alteration rims began before the formation of Fe-Mn crust during the hyperthermal event (Figure 10A).

The opening of the Drake Passage began at approximately 49 Ma in the middle Eocene and continued into the early Miocene (approximately 17 Ma). This period is associated with global cooling, and the Pacific Ocean was affected beginning at approximately 41 Ma (Livermore et al., 2005; Scher and Martin, 2006; Toumoulin et al., 2020). The cold, oxygen-rich, and relatively intensified ocean circulation that resulted from the early opening of the Drake Passage during the middle Eocene may have influenced the paleo-ocean environments of the western Pacific seamounts. Hydrogenetic Fe-Mn crusts are formed by the provision of oxygen-rich seawater to metal ions such as Mn and Fe, which are dissolved in the OMZ. Since the age of L6 was close to 41 Ma (Table 1), the opening of the Drake Passage may have influenced the formation of Fe-Mn crust. However, since the porosity of hydrogenetic Fe-Mn crust is approximately 60% (Conrad et al., 2017; Hein et al., 2017), seawater-basalt interactions likely continued even after the flank became coated with the Fe-Mn crust. Thus, seawater-basalt interactions through the pores in the Fe-Mn crust allowed Fe-smectite formation to continue by maintaining non-vigorous circulation, thereby preventing the dilution of elements dissolved from the basaltic substrate. Therefore, the Fe-smectites in the alteration rims likely formed continuously while oxygenated seawater interacted with basalt under non-vigorous circulations.

4.2.2 Suboxic condition in basaltic substrate

The distinct texture and mineralogy of each layer can be used to illustrate the paleo-ocean environment during the formation of the Fe-Mn crust (Table 1 and Figure 4). The six layers were separated into two groups (L1–4 and L5–6) based on the presence of CFA (Figure 4). The age obtained for L5 (approximately 30.17 Ma), which contained CFA, corresponds with the early Oligocene (Table 1 and Figure 4) and suggests that the Oi-1 glaciation (34–33 Ma) (Viganò et al., 2024) and global phosphatization events influenced L5. At the Eocene-Oligocene boundary (approximately 34 Ma) (Viganò et al., 2024) and the early Oligocene, bottom water temperatures decreased and intensified ocean circulation led to increased surface productivity near seamounts, resulting in a significant increase in phosphate (Hein et al., 1993; Jones et al., 2002). In addition, the sea level drop during this period (Haq et al., 1987) facilitated phosphate transport from land to ocean, thereby promoting phosphatization. CFA, which is produced by phosphatization and was identified in the lower parts of the Fe-Mn crust (Figure 4), is known to impregnate pores, fractures and/or veins in Fe-Mn oxide layers (Hein et al., 2017). The L5 (30.17 Ma) and the upper part of L6 (33.39 Ma) indicate that seawater-basalt interactions weakened owing to impregnation by CFA that formed during the Oi-1 glaciation and global phosphatization events. As a result, the oxygen supply decreased and Fe-smectite formation in the alteration rim was interrupted. In addition, the planktonic foraminifera *G. menardii* observed in the light-yellow matrix of the basaltic substrate (Figure 3B) inhabited the tropical and subtropical oceans during the Cenozoic. The global carbonate compensation depth during the Cenozoic is known to be deeper than approximately 1,500 m (Delaney and Boyle, 1988). Therefore, the foraminifera tests are expected to be preserved above the CCD. Glauconite, which is found in the alteration rim, forms under

organic-rich suboxic conditions via glauconitization, such as in foraminifera tests (Baldermann et al., 2013; Odin, 1988). The glauconitization process requires organic matter, and the seamount underwent a period of expanding OMZ due to increased surface productivity before the formation of Fe-Mn crusts (Hyeong et al., 2013). In other words, the increase in surface productivity likely led to increased organic matter in the water column, which may have resulted in the supply of organic matter. Consequently, organic-rich condition with foraminifera in the basaltic substrate facilitated the formation of glauconite.

The formation of Fe-smectite in the basaltic substrate of the Fe-Mn crust indicates oxic conditions, whereas glauconite indicates suboxic conditions. The authigenic clay minerals identified in the alteration rim indicate different micro-environments, suggesting that the substrate of the Fe-Mn crust used in this study underwent a transition from oxic to suboxic conditions. In this context, authigenic clay minerals can be used as proxies for reconstructing paleo-ocean environments on seamount flanks. Further research on additional samples is needed to enhance the current understanding of changes in oxic-suboxic conditions on the Magellan Seamounts flanks in the western Pacific. The impacts of the opening of the Drake Passage on the formation of secondary minerals in western Pacific seamounts are currently poorly understood. Consequently, these findings could provide a novel proxy for reconstructing paleo-ocean environments on the Magellan Seamounts.

5 Conclusions

In this study, we aimed to reconstruct the paleo-ocean environments on the flanks of seamount KC-7 using secondary minerals in the alteration rims of basaltic substrate associated with the Fe-Mn crust. Mineralogical and biogeochemical analyses of the secondary minerals Fe-smectite and glauconite, which indicate changes in the oxic-suboxic conditions on the seamount flank. First, K-enriched Fe-smectite indicates basalt alteration with the continuous supply of oxygenated seawater. These seawater-basalt interactions likely occurred before the Fe-Mn crusts formed. Despite the Fe-Mn incrustation, seawater-basalt interactions likely continued owing to the high porosity, which sustained Fe-smectite formation. Therefore, the presence of Fe-smectite indicates that the seamount flank experienced oxic conditions during the Cenozoic hyperthermal events (i.e., PETM, EECO, and MECO) and the initial stages of Fe-Mn crust formation (approximately 40.78 Ma). Second, global cooling following the Eocene triggered phosphatization events that precipitated CFA. As a result, CFA impregnated the pores in the Fe-Mn crust and reduced seawater-basalt interactions, which led to partially suboxic condition in the basaltic substrate. Under suboxic condition, glauconite was formed via glauconitization (Fe-smectite-to-glauconite) process. Thus, the presence of glauconite indicates that the seamount flank experienced partially suboxic condition after phosphatization

events during Oi-1 glaciation. In conclusion, the Fe-smectite and glauconite identified in the basaltic substrate associated with the Fe-Mn crust reflect changes in the oxic-suboxic conditions on the seamount flank. The findings of this study suggest that authigenic clay minerals can be used as proxies for reconstructing changes of paleo-ocean environments.

Data availability statement

The original contributions presented in the study are included in the article/Supplementary Material. Further inquiries can be directed to the corresponding author.

Author contributions

HA: Conceptualization, Data curation, Formal Analysis, Methodology, Visualization, Writing – original draft, Writing – review & editing. JJ: Formal Analysis, Validation, Visualization, Writing – review & editing. HH: Data curation, Methodology, Writing – original draft. SK: Data curation, Formal Analysis, Visualization, Writing – review & editing. JK: Methodology, Writing – review & editing. YK: Project administration, Writing – review & editing. KY: Project administration, Supervision, Validation, Writing – original draft, Writing – review & editing.

Funding

The author(s) declare that financial support was received for the research, authorship, and/or publication of this article. This research was a part of a project entitled 'Selection of prospective mining area for Co-rich ferromanganese crust in western Pacific seamounts: 3-D resource estimation and environmental impact evaluation', which was funded by the Korean Ministry of Oceans and Fisheries, Korea (RS-2022-KS221644), the Korea Institute of Marine Science & Technology Promotion (KIMST), the Ministry of Oceans and Fisheries (Reconstruction of the effects of deep ocean currents on sediments through mineralogical and biogeochemical analysis in Magellan Seamount, the Northwest Pacific Ocean, RS-2023-KS231697), the Learning & Academic research institution for Master's-PhD students, and the Postdocs (LAMP) Program of the National Research Foundation of Korea (NRF) grant funded by the Ministry of Education (No. RS-2023-00301938).

Acknowledgments

We are grateful to the reviewers for their constructive feedback on the paper.

Conflict of interest

The authors declare that the research was conducted in the absence of any commercial or financial relationships that could be construed as a potential conflict of interest.

Publisher's note

All claims expressed in this article are solely those of the authors and do not necessarily represent those of their affiliated

organizations, or those of the publisher, the editors and the reviewers. Any product that may be evaluated in this article, or claim that may be made by its manufacturer, is not guaranteed or endorsed by the publisher.

Supplementary material

The Supplementary Material for this article can be found online at: <https://www.frontiersin.org/articles/10.3389/fmars.2024.1481396/full#supplementary-material>

References

- Alt, J. C., and Honnorez, J. (1984). Alteration of the upper oceanic crust, DSDP site 417: mineralogy and chemistry. *Contrib. Mineral. Petrol.* 87, 149–169. doi: 10.1007/BF00376221
- Alt, J. C., Honnorez, J., Laverne, C., and Emmermann, R. (1986). Hydrothermal alteration of a 1 km section through the upper oceanic crust, Deep Sea Drilling Project Hole 504B: Mineralogy, chemistry and evolution of seawater-basalt interactions. *J. Geophys. Res. Solid Earth* 91, 10309–10335. doi: 10.1029/JB091iB10p10309
- Alt, J. C., Lonsdale, P., Haymon, R., and Muehlenbachs, K. (1987). Hydrothermal sulfide and oxide deposits on seamounts near 21°N, East Pacific Rise. *Geol. Soc. Am. Bull.* 98, 157–168. doi: 10.1130/0016-7606(1987)98<157:HSAODO>2.0.CO;2
- Bach, W., and Edwards, K. J. (2003). Iron and sulfide oxidation within the basaltic ocean crust: implications for chemolithoautotrophic microbial biomass production. *Geochim. Cosmochim. Acta* 67, 3871–3887. doi: 10.1016/S0016-7037(03)00304-1
- Baldermann, A., Banerjee, S., Czuppon, G., Dietzel, M., Farkaš, J., Löhr, S., et al. (2022). Impact of green clay authigenesis on element sequestration in marine settings. *Nat. Commun.* 13, 1527. doi: 10.1038/s41467-022-29223-6
- Baldermann, A., Warr, L. N., Grathoff, G. H., and Dietzel, M. (2013). The rate and mechanism of deep-sea glauconite formation at the Ivory Coast–Ghana Marginal Ridge. *Clays Clay Miner.* 61, 258–276. doi: 10.1346/CCMN.2013.0610307
- Benites, M., Hein, J. R., Mizell, K., and Jovane, L. (2021). Miocene phosphatization of rocks from the summit of Rio Grande Rise, Southwest Atlantic Ocean. *Paleoceanogr. Paleoeclimatol.* 36, 24. doi: 10.1029/2020PA004197
- Bernardini, S., Della Ventura, G., Sodo, A., Benites, M., Jovane, L., Hein, J. R., et al. (2022). Micro-Raman mapping of critical metals (Li, Co, Ni) in a rhythmically laminated deep-ocean ferromanganese deposit. *Geochem.* 84, 2. doi: 10.1016/j.chemer.2023.126014
- Böhlke, J., Honnorez, J., and Honnorez-Guerstein, B.-M. (1980). Alteration of basalts from site 396 B, DSDP: Petrographic and mineralogic studies. *Contrib. Mineral. Petr.* 73, 341–364. doi: 10.1007/BF00376628
- Bonatti, E., Kraemer, T., and Rydell, H. (1972). Classification and genesis of submarine iron-manganese deposits, in *Ferromanganese Deposits of the Ocean Floor* (Berlin, Germany: Springer), 149–166.
- Chevrier, V., Poulet, F., and Bibring, J.-P. (2007). Early geochemical environment of Mars as determined from thermodynamics of phyllosilicates. *Nature* 448, 60–63. doi: 10.1038/nature05961
- Clayton, T., and Pearce, R. (2000). Alteration mineralogy of Cretaceous basalt from ODP site 1001, Leg 165 (Caribbean Sea). *Clay Miner.* 35, 719–733. doi: 10.1180/000985500547043
- Coccatto, A., Bersani, D., Coudray, A., Sanyova, J., Moens, L., and Vandenberghe, P. (2016). Raman spectroscopy of green minerals and reaction products with an application in Cultural Heritage research. *J. Raman Spectrosc.* 47, 1429–1443. doi: 10.1002/jrs.4956
- Conrad, T., Hein, J. R., Paytan, A., and Clague, D. A. (2017). Formation of Fe-Mn crusts within a continental margin environment. *Ore Geol. Rev.* 87, 25–40. doi: 10.1016/j.oregeorev.2016.09.010
- Cuadros, J., Dekov, V. M., Arroyo, X., and Nieto, F. (2011). Smectite formation in submarine hydrothermal sediments: Samples from the HMS Challenger expedition, (1872–1876). *Clays Clay Miner.* 59, 164–164. doi: 10.1346/CCMN.2011.0590204
- Dekov, V. M., Cuadros, J., Shanks, W. C., and Koski, R. A. (2008). Deposition of talc–kerolite-smectite–smectite at seafloor hydrothermal vent fields: Evidence from mineralogical, geochemical and oxygen isotope studies. *Chem. Geol.* 247, 171–194. doi: 10.1016/j.chemgeo.2007.10.022
- Delaney, M. L., and Boyle, E. A. (1988). Tertiary paleoceanic chemical variability: Unintended consequences of simple geochemical models. *Paleoceanography* 3, 137–156. doi: 10.1029/PA003i002p0137
- Duncan, R. A., and Clague, D. A. (1985). “Pacific plate motion recorded by linear volcanic chains,” in *The ocean basins and margins* (Boston, MA: Springer).
- Edwards, K. J., Bach, W., and Mccollom, T. M. (2005). Geomicrobiology in oceanography: microbe–mineral interactions at and below the seafloor. *Trends Microbiol.* 13, 449–456. doi: 10.1016/j.tim.2005.07.005
- Ehrmann, W. U., and Mackensen, A. (1992). Sedimentological evidence for the formation of an East Antarctic ice sheet in Eocene/Oligocene time. *Paleoecol. Palaeoclimatol. Palaeoecol.* 93, 85–112. doi: 10.1016/0031-0182(92)90185-8
- Eriksen, C. C. (1991). Observations of amplified flows atop a large seamount. *J. Geophys. Res. Oceans* 96, 15227–15236. doi: 10.1029/91JC01176
- Frost, R. L., and Klopogge, J. T. (2000). Raman spectroscopy of nontronites. *Appl. Spectrosc.* 54, 402–405. doi: 10.1366/0003702001949483
- Giorgioni, M., Jovane, L., Rego, E. S., Rodelli, D., Frontalini, F., Coccioni, R., et al. (2019). Carbon cycle instability and orbital forcing during the Middle Eocene Climate Optimum. *Sci. Rep.* 9, 9357. doi: 10.1038/s41598-019-45763-2
- Giresse, P., and Wiewióra, A. (2001). Stratigraphic condensed deposition and diagenetic evolution of green clay minerals in deep water sediments on the Ivory Coast–Ghana Ridge. *Mar. Geol.* 179, 51–70. doi: 10.1016/S0025-3227(01)00193-1
- Glasby, G. P., Ren, X., Shi, X., and Pulyaeva, I. A. (2007). Co-rich Mn crusts from the Magellan Seamount cluster: the long journey through time. *Geo-Mar. Lett.* 27, 315–323. doi: 10.1007/s00367-007-0055-5
- Halbach, P., and Puteanus, D. (1984). The influence of the carbonate dissolution rate on the growth and composition of Co-rich ferromanganese crusts from Central Pacific seamount areas. *Earth. Planet. Sci. Lett.* 68, 73–87. doi: 10.1016/0012-821X(84)90141-9
- Haq, B. U., Hardenbol, J., and Vail, P. R. (1987). Chronology of fluctuating sea levels since the Triassic. *Science* 235, 1156–1167. doi: 10.1126/science.235.4793.1156
- Hein, J. R., Koschinsk, A., Bau, M., Manheim, F. T., Kang, J.-K., and Roberts, L. (2017). “Cobalt-rich ferromanganese crusts in the Pacific,” in *Handbook of marine mineral deposits* (London, UK: Routledge).
- Hein, J. R., Yeh, H.-W., and Alexander, E. (1979). Origin of iron-rich montmorillonite from the manganese nodule belt of the north equatorial Pacific. *Clays clay miner.* 27, 185–194. doi: 10.1346/CCMN.1979.0270303
- Hein, J. R., Yeh, H. W., Gunn, S. H., Sliter, W. V., Benninger, L. M., and Wang, C. H. (1993). Two major Cenozoic episodes of phosphogenesis recorded in equatorial Pacific seamount deposits. *Paleoceanography* 8, 293–311. doi: 10.1029/93PA00320
- Hurst, V. J., Schroeder, P. A., and Styron, R. W. (1997). Accurate quantification of quartz and other phases by powder X-ray diffractometry. *Anal. Chim. Acta* 337, 233–252. doi: 10.1016/S0003-2670(96)00425-4
- Hutchinson, D. K., Coxall, H. K., Lunt, D. J., Steinthorsdottir, M., De Boer, A. M., Baatsen, M., et al. (2021). The Eocene-Oligocene transition: a review of marine and terrestrial proxy data, models and model-data comparisons. *Clim. Past* 17, 269–315. doi: 10.5194/cp-17-269-2021
- Hyeong, K., Kim, J., Yoo, C. M., Moon, J.-W., and Kim, K.-H. (2008). Phosphogenesis recorded in the Co-rich crusts of the northwest Pacific seamounts. *J. Geol. Soc. Korea* 44, 435–446.
- Hyeong, K., Kim, J., Yoo, C. M., Moon, J.-W., and Seo, I. (2013). Cenozoic history of phosphogenesis recorded in the ferromanganese crusts of central and western Pacific seamounts: Implications for deepwater circulation and phosphorus budgets. *Paleoecol. Palaeoclimatol. Palaeoecol.* 392, 293–301. doi: 10.1016/j.palaeo.2013.09.012
- Jarrard, R. D. (2003). Subduction fluxes of water, carbon dioxide, chlorine, and potassium. *Geochem. Geophys. Geosyst.* 4, 8905. doi: 10.1029/2002GC000392
- Jones, E., Boudagher-Fadel, M., and Thirlwall, M. (2002). An investigation of seamount phosphorites in the Eastern Equatorial Atlantic. *Mar. Geol.* 183, 143–162. doi: 10.1016/S0025-3227(01)00254-7

- Jung, J., Hyeong, K., Kim, J. H., Kim, J., Ko, Y., Yang, K., et al. (2022). Latitudinal changes in elemental composition of smectite in deep sea sediments and its implication for microbial activity along the transect of equatorial Pacific Ocean. *Appl. Clay Sci.* 229, 106672. doi: 10.1016/j.clay.2022.106672
- Kim, S., An, H., Kim, C., and Yang, K. (2023). Mineralogy, geochemistry, and sources of clay minerals in sediments of the Ulleung Basin, East Sea (Sea of Japan). *Geosci. J.* 27 (4), 385–397. doi: 10.1007/s12303-023-0011-z
- Kim, J., Hyeong, K., Jung, H. S., Moon, J. W., Kim, K. H., and Lee, I. (2006). Southward shift of the Intertropical Convergence Zone in the western Pacific during the late Tertiary: Evidence from ferromanganese crusts on seamounts west of the Marshall Islands. *Paleoceanography* 21, 1–14. doi: 10.1029/2006PA001291
- Knowles, E., Wirth, R., and Templeton, A. (2012). A comparative analysis of potential biosignatures in basalt glass by FIB-TEM. *Chem. Geol.* 330, 165–175. doi: 10.1016/j.chemgeo.2012.08.028
- Koschinsky, A., and Hein, J. R. (2017). Marine ferromanganese encrustations: archives of changing oceans. *Elements: Int. Magazine Mineralogy Geochemistry Petrology* 13, 177–182. doi: 10.2113/gselements.13.3.177
- Livemore, R., Nankivell, A., Eagles, G., and Morris, P. (2005). Paleogene opening of Drake passage. *Earth. Planet. Sc. Lett.* 236, 459–470. doi: 10.1016/j.epsl.2005.03.027
- Logvinenko, N. (1982). Origin of glauconite in the recent bottom sediments of the ocean. *Sediment. Geol.* 31, 43–48. doi: 10.1016/0037-0738(82)90006-9
- López-Quirós, A., Escutia, C., Sánchez-Navas, A., Nieto, F., Garcia-Casco, A., Martín-Algarra, A., et al. (2019). Glaucony authigenesis, maturity and alteration in the Weddell Sea: An indicator of paleoenvironmental conditions before the onset of Antarctic glaciation. *Sci. Rep.* 9, 1–12. doi: 10.1038/s41598-019-50107-1
- López-Quirós, A., Sánchez-Navas, A., Nieto, F., and Escutia, C. (2020). New insights into the nature of glauconite. *Am. Mineral.* 105, 674–686. doi: 10.2138/am-2020-7341
- Manheim, F. T., and Lane-Bostwick, C. M. (1988). Cobalt in ferromanganese crusts as a monitor of hydrothermal discharge on the Pacific sea floor. *Nature* 335, 59–62. doi: 10.1038/335059a0
- Marinoni, L., Setti, M., Salvi, C., and Lopez-Galindo, A. (2008). Clay minerals in late Quaternary sediments from the south Chilean margin as indicators of provenance and paleoclimate. *Clay Miner.* 43, 235–253. doi: 10.1180/claymin.2008.043.2.07
- McClain, C. R. (2007). Seamounts: identity crisis or split personality? *J. Biogeogr.* 34 (12), 2001–2008. doi: 10.1111/j.1365-2699.2007.01783.x
- Melnikov, M. E., and Pletnev, S. P. (2013). Age and formation conditions of the Co-rich manganese crust on guyots of the Magellan seamounts. *Lithol. Miner. Resour.* 48, 1–13. doi: 10.1134/S0024490212050057
- Melson, W. G., and Thompson, G. (1973). Glassy abyssal basalts, Atlantic sea floor near St. Paul's Rocks: petrography and composition of secondary clay minerals. *Geol. Soc. Am. Bull.* 84, 703–716. doi: 10.1130/0016-7606(1973)84<703:GABASF>2.0.CO;2
- Menard, H. (1984). Darwin reprise. *J. Geophys. Res. Solid Earth* 89, 9960–9968. doi: 10.1029/JB089iB12p09960
- Meunier, A. (2005). *Clays* (Germany: Springer Science & Business Media).
- Moon, J. W. (2016). *Exploration for Seafloor Hydrothermal Deposits and Fe-Mn Crusts in the Southwestern Pacific and the Indian Ocean*. (South Korea: Ministry of Oceans and Fisheries). p. 147–149.
- Odin, G. S. (1988). *Green marine clays: oolitic ironstone facies, verdine facies, glaucony facies and celadonite-bearing rock facies—a comparative study* (Elsevier).
- Odin, G. S., and Matter, A. (2003). De glauconiarum origine. *Sandstone diagenesis: Recent ancient* (Hoboken, New Jersey, USA: Wiley) 28, 121–151. doi: 10.1002/9781444304459.ch4
- Park, J., Jung, J., Ko, Y., Lee, Y., and Yang, K. (2023). Reconstruction of the Paleocene environment using mineralogical and geochemical analyses of mixed-type ferromanganese nodules from the tabletop of Western Pacific Magellan Seamount. *Geochim. Geophys. Geosyst.* 24 (2). doi: 10.1029/2022GC010768
- Pelletier, E., Fouquet, Y., Etoubleau, J., Cheron, S., Josso, P., Labanieh, S., et al. (2015). The nickel-, copper-, cobalt-rich hydrothermal manganese deposits from the Wallis and Futuna area, SW Pacific. SGA 2015: 13th SGA Biennial Meeting; Nancy, France.
- Pichler, T., Ridley, W. I., and Nelson, E. (1999). Low-temperature alteration of dredged volcanics from the Southern Chile Ridge: additional information about early stages of seafloor weathering. *Mar. Geol.* 159, 155–177. doi: 10.1016/S0025-3227(99)00008-0
- Pitcher, T. J., Morato, T., Hart, P. J., Clark, M. R., Haggan, N., and Santos, R. S. (2007). *Seamounts: ecology, fisheries & conservation* (Hoboken, New Jersey, USA: Wiley Online Library).
- Puteanus, D., and Halbach, P. (1988). Correlation of Co concentration and growth rate—A method for age determination of ferromanganese crusts. *Chem. Geol.* 69, 73–85. doi: 10.1016/0009-2541(88)90159-3
- Ramos, D. P. S., Coogan, L. A., Murphy, J. G., and Higgins, J. A. (2020). Low-temperature oceanic crust alteration and the isotopic budgets of potassium and magnesium in seawater. *Earth. Planet. Sci. Lett.* 541, 116290. doi: 10.1016/j.epsl.2020.116290
- Scher, H. D., and Martin, E. E. (2006). Timing and climatic consequences of the opening of Drake Passage. *science* 312, 428–430. doi: 10.1126/science.1120044
- Scotese, C. R., Song, H., Mills, B. J., and van der Meer, D. G. (2021). Phanerozoic paleotemperatures: The earth's changing climate during the last 540 million years. *Earth Sci. Rev.* 215, 103503. doi: 10.1016/j.earscirev.2021.103503
- Shao, Q., Chen, X., and Huang, R. (2013). Effect of opening the Drake Passage on the oceanic general circulation: A box model study. *Sci. China Earth Sci.* 56, 1588–1598. doi: 10.1007/s11430-012-4571-4
- Singh, P., Banerjee, S., Choudhury, T. R., Bhattacharya, S., and Pande, K. (2023). Distinguishing celadonite from glauconite for environmental interpretations: a review. *J. Palaeogeogr.* 12, 179–194. doi: 10.1016/j.jop.2023.02.001
- Song, H., Wignall, P. B., Song, H., Dai, X., and Chu, D. (2019). Seawater temperature and dissolved oxygen over the past 500 million years. *J. Earth Sci.* 30, 236–243. doi: 10.1007/s12583-018-1002-2
- Toumoulin, A., Donnadieu, Y., Ladant, J. B., Batenburg, S., Poblete, F., and Dupont-Nivet, G. (2020). Quantifying the effect of the Drake Passage opening on the Eocene Ocean. *Paleoceanogr. Paleoclimatol.* 35, 1–22. doi: 10.1029/2020PA003889
- Tripathi, A., and Elderfield, H. (2005). Deep-sea temperature and circulation changes at the Paleocene-Eocene thermal maximum. *Science* 308, 1894–1898. doi: 10.1126/science.1109202
- Viganò, A., Dallanave, E., Alegret, L., Westerhold, T., Sutherland, R., Dickens, G. R., et al. (2024). Calcareous nannofossils and paleoclimatic evolution across the Eocene-Oligocene transition at IODP Site U1509, Tasman Sea, Southwest Pacific Ocean. *Paleoceanogr. Paleoclimatol.* 39, 1–23. doi: 10.1029/2023PA004738
- Weaver, C. E. (1989). *Clays, muds, and shales* (Amsterdam, Netherlands: Elsevier).
- Wessel, P., and Kroenke, L. W. (1998). The geometric relationship between hot spots and seamounts: Implications for Pacific hot spots. *Earth. Planet. Sci. Lett.* 158, 1–18. doi: 10.1016/S0012-821X(98)00043-0
- Wilson, M. (1999). The origin and formation of clay minerals in soils: past, present and future perspectives. *Clay miner.* 34, 7–25. doi: 10.1180/000985599545957
- Winguth, A. M., Thomas, E., and Winguth, C. (2012). Global decline in ocean ventilation, oxygenation, and productivity during the Paleocene-Eocene Thermal Maximum: Implications for the benthic extinction. *Geology* 40, 263–266. doi: 10.1130/G32529.1
- Wu, G., Zhou, H., Zhang, H., Ling, H., Ma, W., Zhao, H., et al. (2007). New index of ferromanganese crusts reflecting oceanic environmental oxidation. *Sci. China Ser. D* 50, 371–384. doi: 10.1007/s11430-007-2011-7
- Yamashita, S., Mukai, H., Tomioka, N., Kagi, H., and Suzuki, Y. (2019). Iron-rich smectite formation in subseafloor basaltic lava in aged oceanic crust. *Sci. Rep.* 9, 11306. doi: 10.1038/s41598-019-47887-x
- Yang, K., Kim, J.-W., Kogure, T., Dong, H., Baik, H., Hoppie, B., et al. (2016). Smectite, illite, and early diagenesis in South Pacific Gyre subseafloor sediment. *Appl. Clay Sci.* 134, 34–43. doi: 10.1016/j.clay.2016.03.041
- Yang, K., Park, H., Baik, H., Kogure, T., and Kim, J. (2018). The formation of Fe-bearing secondary phase minerals from the basalt—Sediment interface, South Pacific gyre: IODP expedition 329. *Clays Clay Miner.* 66, 1–8. doi: 10.1346/CCMN.2018.064083
- Yang, K., Park, H., Son, S.-K., Baik, H., Park, K., Kim, J., et al. (2019). Electron microscopy study on the formation of ferromanganese crusts, western Pacific Magellan Seamounts. *Mar. Geol.* 410, 32–41. doi: 10.1016/j.margeo.2019.01.001
- Zeebe, R. E. (2013). What caused the long duration of the Paleocene-Eocene Thermal Maximum? *Paleoceanography* 28, 440–452. doi: 10.1002/palo.20039